Voltage Signatures between Two Sub–Windings in Dual Three-Phase Induction Motor under Static Air-Gap Eccentricity

Y. MAOUCHE, M.E.K. OUMAAMAR, A. L. NEMMOUR, A. KHEZZAR

Laboratoire d'électrotechnique de Constantine
Département d'électrotechnique
Université Constantine 1, 25000, Constantine, Algeria
yassine.maouche@lec-umc.org

Abstract

The present paper focuses on the analysis of a new diagnostic method based on frequency analysis of voltage between two sub-windings in dual three-phase induction motor. The possibility to extract diagnosis signatures of static eccentricity is investigated. The used model of squirrel cage induction machine takes into account the geometry and the winding layout in order to analyze the impact of the static eccentricity and to predict the related frequencies on the voltage between two sub-windings of the motor. The simulation results and analytical developpement show the effectiveness of the method. Experimental results are provided to underpin the theoretical considerations.

1. Introduction

In the last years the interest in multi-phase induction motor has grown, extensively discussed is the six-phase induction motor. The increasing of phase number of stator winding which means decreasing of an angle shift among phases have potential advantages such as reducing torque pulsation, joule losses and greater fault tolerance in open phases [1]-[4]. The dual three-phase motor as the three-phase one can be submitted to external and internal stresses of various natures which cause different faults and degradation in its performances. Many methods have been proposed to diagnose these faults [5]-[10], especially the static eccentricity which contributes toward a considerable percentage of induction machine failures. One can underline the analysis of the Fourier spectrum stator current MSCA, the use of electromagnetic flux measured by coils sensing the axial leakage flux, the vibration and the air gap torque measurement.

The dual three-phase induction motor is most frequently configured with two sub-windings shifted by $0°$, $30°$ and $60°$ electrical degrees and two isolated neutral points. The impact of winding with a single neutral point has been investigated in [11] but the possibility to extract diagnostic signatures using voltage between sub-windings of dual-three phase induction motor is not presented. For that, the aim of the present paper is to extend the analysis presented in [12] so as to consider the multiplication of the number of phases. The harmonic content of the voltage between sub-windings of motor of healthy motor is analytically investigated and extended to the constructional rotor bar and/ or static eccentricity failure cases.
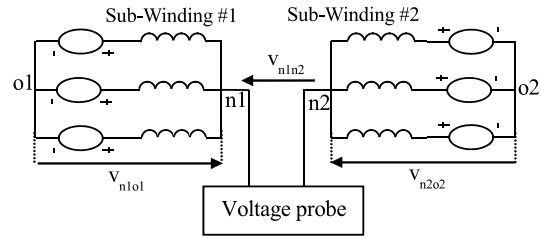

Figure 1. Simulation and Experimental setup for calculation and measuring of voltage between winding-set of motor.

2. Analysis model of dual three-phase induction motor

The dual three-phase induction motor considered having two isolated neutral is shown in Fig. 1. Suppose that the two stator sets of dual three windings sets are Y connected. The rotor cage having n_b bars is viewed as n_b identical spaced loops, and the current distribution can be specified in terms of $n_b + 1$ independent rotor currents.

The primary equations of the dual three-phase induction motor can be written in vector–matrix form as follows:

$$[v_s] = [R_s] \cdot [I] + \frac{d}{dt}[\psi_s] + [V_n] \qquad (1)$$

$$\begin{bmatrix} [V_r] \\ V_e \end{bmatrix} = [0] = \begin{bmatrix} [R_r] & & \frac{R_e}{n_b} \\ & & \vdots \\ \frac{R_e}{n_b} & \cdots & R_e \end{bmatrix} \begin{bmatrix} [i_r] \\ i_e \end{bmatrix} \qquad (2)$$
$$+ \frac{d}{dt}[\psi_r]$$

$$[\psi_s] = [L_s][i_s] + [M_{sr}][i_r] \qquad (3)$$

$$\begin{bmatrix} [\psi_r] \\ \psi_e \end{bmatrix} = \begin{bmatrix} [M_{sr}] \cdot [i_s] \\ 0 \end{bmatrix} \qquad (4)$$
$$+ \begin{bmatrix} [L_r] & & \frac{L_e}{n_b} \\ & & \vdots \\ \frac{L_e}{n_b} & \cdots & L_e \end{bmatrix} \cdot \begin{bmatrix} [i_r] \\ i_e \end{bmatrix}$$

where:

$$[v_s] = \begin{bmatrix} v_{sa} & v_{sb} & v_{sc} & v_{sd} & v_{se} & v_{sf} \end{bmatrix}^t$$

$$[I_s] = \begin{bmatrix} I_{sa} & I_{sb} & I_{sc} & I_{sd} & I_{se} & I_{sf} \end{bmatrix}^t$$

$$[\psi_s] = \begin{bmatrix} \psi_{sa} & \psi_{sb} & \psi_{sc} & \psi_{sd} & \psi_{se} & \psi_{sf} \end{bmatrix}^t$$

are the stator voltages, current and flux vectors respectively.

$$[V_r] = [0] = \begin{bmatrix} V_{r1} & \cdots & V_{rn_b} \end{bmatrix}^t,$$

$$[i_r] = \begin{bmatrix} i_{r1} & \cdots & i_{rn_b} \end{bmatrix}^t,$$

$$[\psi_r] = \begin{bmatrix} \psi_{r1} & \cdots & \psi_{rn_b} \end{bmatrix}^t$$ are the rotor voltages, current and flux linkage vectors, respectively with dimensions $1 \times n_b$. $[R_s]$ and $[R_r]$ are the stator and rotor resistance matrices. $[L_s]$ and $[L_r]$ are the stator and rotor inductance matrices and are described by the same manner as in [9].

$$V_n = \begin{bmatrix} V_{o1n1} & V_{o1n1} & V_{o1n1} & V_{o2n2} & V_{o2n2} & V_{o2n2} \end{bmatrix}^t$$

is the line neutral voltage taking place between the supply sets and the stator sets neutral is given by:

$$V_{o1n1} = \frac{1}{3}(V_{sa} + V_{sb} + V_{sc})$$

$$V_{o2n2} = \frac{1}{3}(V_{sd} + V_{se} + V_{sf})$$

We suppose that the voltage between two supplies sets is neglected. The voltage between stator sets of dual three windings is defined by:

$$V_{n1n2} = V_{o1n1} - V_{o2n2} \tag{5}$$

As there is no method to infer it, we have to set the stator equations of the model in line-to-line voltage form:

$$\begin{bmatrix} V_{sab} \\ V_{sbc} \\ V_{sde} \\ V_{sef} \end{bmatrix} = \begin{bmatrix} R_s & -R_s & 0 & 0 \\ R_s & 2R_s & 0 & 0 \\ 0 & 0 & R_s & -R_s \\ 0 & 0 & R_s & 2R_s \end{bmatrix} \cdot \begin{bmatrix} I_{sa} \\ I_{sb} \\ I_{sd} \\ I_{se} \end{bmatrix}$$

$$+ \frac{d}{dt} \begin{bmatrix} \psi_{sa} \\ \psi_{sb} \\ \psi_{sd} \\ \psi_{se} \end{bmatrix} \tag{6}$$

The zero sequence components corresponding to each stator sets are defined by:

$$\begin{cases} v_{sa} + v_{sb} + v_{sc} = 3v_{so1} \\ v_{sd} + v_{se} + v_{sf} = 3v_{so2} \end{cases} \tag{7}$$

The zero sequence components of supply voltage corresponding to each stator sets are phase-shifted by α electrical degrees. From the summation of matrix lines of (6) and by using (5) and (7) we get:

$$V_{n1n2} = \frac{1}{3}\frac{d}{dt}(\psi_{sd} + \psi_{se} + \psi_{sf} - \psi_{sa} - \psi_{sb} - \psi_{sc}) + v_{so1} - v_{so2} \tag{8}$$

The mutual inductance is calculated using winding function approach includes all the space and rotor harmonics in the machine, its development into Fourier series is given by (9) in the bottom of this page.

3. Voltage between dual three-phase induction motor in healthy condition

When a dual three-phase induction motor is feed by a symmetrical voltage system a forward rotating field is induced in its air gap. The rotor currents which flow in the rotor loops as a result of the forward field can be expressed as:

$$[i_{rpk}] = \begin{bmatrix} \vdots \\ I_{rpk} \cos(gw_s t - ka - \gamma_p) \\ \vdots \end{bmatrix} \tag{10}$$

where g is the slip, γ_p is the initial phase angle and I_{rpk} is the maximum value of the k rotor loop current.

From (8) and (10) and by substituting θ by $(1-g)w_s t + \theta_0$ we get:

$$V_{n1n2} = \sum_{h}^{\infty} \sum_{k=0}^{n_b} M_{sr}^{3h} I_{rpk} \left\{ \frac{3h}{2}\frac{d\theta}{dt} + \frac{g\omega_s}{2} \right\} \times$$
$$\left[\sin(\theta_{3h-1}^{(1)}) - \sin(\theta_{3h-1}^{(1)} + 3h\alpha) \right]$$
$$+ \sum_{h}^{\infty} \sum_{k=0}^{n_b} M_{sr}^{3h} I_{rpk} \left\{ \frac{3h}{2}\frac{d\theta}{dt} - \frac{g\omega_s}{2} \right\} \times$$
$$\left[\sin(\theta_{3h+1}^{(1)}) - \sin(\theta_{3h+1}^{(1)} + 3h\alpha) \right] \tag{11}$$

where:
$$\theta_{3h-1}^{(1)} = (3h - (3h-1)g)\omega_s t + 3h(\phi_h + \theta_0) + (3h-1)ka$$
$$\theta_{3h+1}^{(1)} = (3h - (3h+1)g)\omega_s t + 3h(\phi_h + \theta_0) + (3h+1)ka$$

The relation (11) shows that V_{n1n2} is equal to zero except when h belongs to the following set:

$$F = \left\{ h = (6k \pm 1)_{k=1,2...} \cap h = \frac{1}{3}(\lambda \frac{n_b}{p} \pm 1)_{\lambda=1,2...} \right\} \tag{12}$$

Under these conditions, the harmonic components in V_{n1n2} have a series of high-frequency components induced by the space distribution of rotor bars given by the following expression:

$$\begin{cases} f_{sh}(3h) = (3h - (3h-1)g)f_s & \text{when} \quad h = \frac{1}{3}(\lambda \frac{n_b}{p} + 1) \\ f_{sh}(3h) = (3h - (3h+1)g)f_s & \text{when} \quad h = \frac{1}{3}(\lambda \frac{n_b}{p} - 1) \end{cases} \tag{13}$$

Figure 2 shows the spectral content of the voltage between sub-winding of dual three-phase induction motor under healthy condition. Calculations were made using MATLAB simulation software for dual three-phase 1.5-kW motor with 24 stator and 22 rotor slots, 1 pair poles, and $g = 0.03$. In the case of $\lambda = 1$, as predicted by (12) and (13), the first RSH which appears in the voltage between sub-windings of motor spectrum is related to the harmonic order 21 for $\lambda = 1$ at frequency $f_{sh}(21) = (21 - 22g)f_s$. The second one is related to the harmonic order 45 for $\lambda = 2$ where $f_{sh}(45) = (45 - 44g)f_s$.

$$[M_{sr}] = \sum_{h=1}^{\infty} M_{sr}^h \times \begin{bmatrix} \cos(h(\theta + \phi_h)) & \cdots & \cos(h(\theta + \phi_h + ka)) & \cdots \\ \cos(h(\theta + \phi_h - \alpha)) & \cdots & \cos(h(\theta + \phi_h + ka - \alpha)) & \cdots \\ \cos(h(\theta + \phi_h - \frac{2\pi}{3})) & \cdots & \cos(h(\theta + \phi_h + ka - \frac{2\pi}{3})) & \cdots \\ \cos(h(\theta + \phi_h - \frac{2\pi}{3} - \alpha)) & \cdots & \cos(h(\theta + \phi_h + ka - \frac{2\pi}{3} - \alpha)) & \cdots \\ \cos(h(\theta + \phi_h + \frac{2\pi}{3})) & \cdots & \cos(h(\theta + \phi_h + ka + \frac{2\pi}{3})) & \cdots \\ \cos(h(\theta + \phi_h + \frac{2\pi}{3} - \alpha)) & \cdots & \cos(h(\theta + \phi_h + ka + \frac{2\pi}{3} - \alpha)) & \cdots \end{bmatrix} \tag{9}$$

where $a = p(2\pi/n_b)$ is the electrical angle of a rotor loop. ϕ_h is the initial phase angle. $k = 1 \cdots n_b$ is a counter of a rotor loop
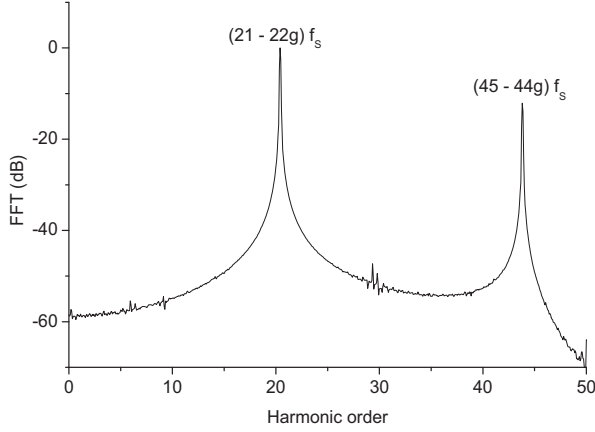
Figure 2. Simulated normalized FFT spectrum of voltage between sub-windings of dual three-phase induction motor in healthy condition.

4. Voltage between two sub-winding of dual three-phase with rotor constructional dissymmetry

4.1. Uniform air-gap

The rotor construction dissymmetry imposes an inequality of the maximum values of the rotor loop witch induces a new series of components of rotor slot harmonics. In this case, additional harmonic components show up at frequencies:

$$f_{sh}(3h) = (3h - (3h \pm 1)g)f_s \tag{14}$$

The speed ripples caused by the rotor dissymmetry induces other frequencies specified by:

$$f_{sh}(3h, k) = (3h - (3h \pm 1)g \pm 2kg)f_s \tag{15}$$

Figure 3 shows the spectral content on the voltage between sub- winding of motor under rotor construction dissymmetry and balanced supply voltage. Additional harmonics described by (14) and (15) bring up and their frequencies are:
$f_{sh}(3, k) = \{\ 2.92f_s, \quad 2.88f_s, \quad 8.76f_s \quad 8.70f_s, \quad \dots \}$

4.2. Non-uniform static air-gap eccentricity

Static eccentricity is unequal air gap between the stator and the rotor caused by a displacement of the axis of rotation where the position of the minimal air gap length is constant in the space. By considering this asymmetrical, additional component of the mutual inductance is added and can be presented into Fourier series as shown (16) (see the bottom of this page). Only the rotor flux given by (4) is needed to describe the additional harmonics in the rotor currents due to the appearance of static air-gap eccentricity:

$$[i_{rek}] = \begin{bmatrix} \vdots \\ I_{rek}\cos((\frac{1-g}{p} - g)w_s t - ka - \gamma_p) \\ \vdots \end{bmatrix} \tag{17}$$

I_{rek} is the maximum value of the k rotor loop current induced by the interaction between stator current and additional mutual inductance induced by the occurrence of static air gap eccentricity (16).

The first additional voltage between sub-windings of dual three-phase induction motor related to the interaction between the healthy part of mutual inductance (9) and the rotor current (17) can be written as:

$$V_{ne1ne2} = \sum_{h}^{\infty} \sum_{k=0}^{n_b} M_{sr}^{3h} I_{rek} \left\{ \frac{3h}{2}\frac{d\theta}{dt} + \frac{(\frac{1-g}{p} - g)w_s}{2} \right\} \times$$
$$\left[\sin\left(\theta_{3h+1}^{(2)}\right) - \sin\left(\theta_{3h+1}^{(2)} + 3h\alpha\right) \right]$$
$$+ \sum_{h}^{\infty} \sum_{k=0}^{n_b} M_{sr}^{3h} I_{rek} \left\{ \frac{3h}{2}\frac{d\theta}{dt} - \frac{(\frac{1-g}{p} - g)w_s}{2} \right\} \times$$
$$\left[\sin\left(\theta_{3h-1}^{(2)}\right) - \sin\left(\theta_{3h-1}^{(2)} + 3h\alpha\right) \right] \tag{18}$$

where:

$$\theta_{3h-1}^{(2)} = (3h-(3h-1)g-\tfrac{1-g}{p})w_s t+3h(\phi_h+\theta_0)+(3h+1)ka$$
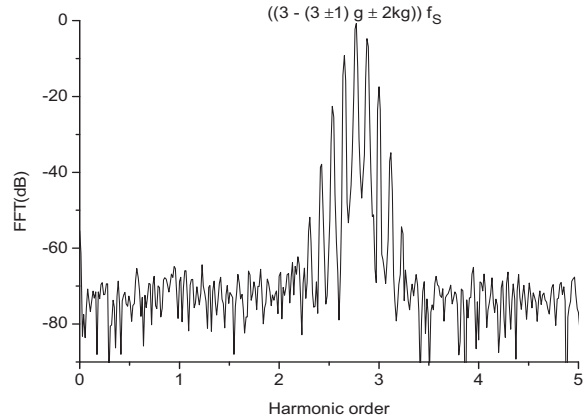$$\theta_{3h+1}^{(2)} = (3h-(3h+1)g+\tfrac{1-g}{p})w_s t+3h(\phi_h+\theta_0)+(3h-1)ka$$

Figure 3. Simulated normalized FFT spectrum of voltage between sub-windings of dual three-phase induction motor with rotor construction dissymmetry.

$$\left[M_{sr}^{(hp+1)}\right] = \sum_{h=1}^{\infty} M_{sr}^{(hp+1)} \begin{bmatrix} \cos((hp+1)(\theta+\phi_h)) & \cdots & \cos((hp+1)(\theta+\phi_h+ka)) & \cdots \\ \cos((hp+1)(\theta+\phi_h-\alpha)) & \cdots & \cos((hp+1)(\theta+\phi_h+ka-\alpha)) & \cdots \\ \cos((hp+1)(\theta+\phi_h-\frac{2\pi}{3})) & \cdots & \cos((hp+1)(\theta+\phi_h+ka-\frac{2\pi}{3})) & \cdots \\ \cos((hp+1)(\theta+\phi_h-\frac{2\pi}{3}-\alpha)) & \cdots & \cos((hp+1)(\theta+\phi_h+ka-\frac{2\pi}{3}-\alpha)) & \cdots \\ \cos((hp+1)(\theta+\phi_h+\frac{2\pi}{3})) & \cdots & \cos((hp+1)(\theta+\phi_h+ka+\frac{2\pi}{3})) & \cdots \\ \cos((hp+1)(\theta+\phi_h+\frac{2\pi}{3}-\alpha)) & \cdots & \cos((hp+1)(\theta+\phi_h+ka+\frac{2\pi}{3}-\alpha)) & \cdots \end{bmatrix} \tag{16}$$

The second additional voltage between sub-windings of dual three-phase induction motor related to the interaction between the faulty part of mutual inductance (16) and the rotor current (17) can be written as:

$$V_{e1e2} = \sum_{h}^{\infty} \sum_{k=0}^{n_b} M_{sr}^{3(hp+1)} I_{rpk} \left\{ \frac{3(hp+1)}{2} \frac{d\theta}{dt} + \left(\frac{1-g}{p} - g \right) \right\} \times$$
$$\left[\sin \left(\theta_{h+1}^{(3)} \right) - \sin \left(\theta_{h+1}^{(3)} + 3(hp+1)\alpha \right) \right]$$
$$+ \sum_{h}^{\infty} \sum_{k=0}^{n_b} M_{sr}^{3(hp+1)} I_{rpk} \left\{ \frac{3(hp+1)}{2} \frac{d\theta}{dt} - \left(\frac{1-g}{p} - g \right) \right\} \times$$
$$\left[\sin \left(\theta_{h-1}^{(3)} \right) - \sin \left(\theta_{h-1}^{(3)} + 3(hp+1)\alpha \right) \right]$$

$$(19)$$

where:
$$\theta_{h+1}^{(3)} = \left(3(hp+1) - (3(hp+1)+1)g + \frac{1-g}{p} \right) w_s t +$$
$$3(hp+1)(\phi_h + \theta_0) + (3(hp+1)-1)ka$$
$$\theta_{h-1}^{(3)} = \left(3(hp+1) - (3(hp+1)-1)g - \frac{1-g}{p} \right) w_s t +$$
$$3(hp+1)(\phi_h + \theta_0) + (3(hp+1)+1)ka$$

The impact of the interaction between the faulty part of mutual inductance (16) and the rotor current (17) in voltage between sub-windings of dual three-phase induction motor is not mentioned due to similarity at frequencies characterizing the rotor construction asymmetry.

Those added voltage components (16) and (19) give additional harmonics with the following frequencies without consideration of speed ripple effect caused by rotor asymmetry:

$$f_{sh}(3h) = (3h - (3h \pm 1)g \pm \frac{1-g}{p})f_s \qquad (20)$$

$$f_{sh}(3(hp+1)) = (3(hp+1) - (3(hp+1) \pm 1)g \pm \frac{1-g}{p})f_s$$
$$(21)$$

and with consideration of speed ripple effect caused by rotor asymmetry :

$$f_{sh}(3h, k) = (3h - (3h \pm 1)g \pm \frac{1-g}{p} \pm 2kg)f_s \qquad (22)$$

$$f_{sh}(3(hp+1), k) = \left(3(hp+1) - (3(hp+1) \pm 1)g \right. \qquad (23)$$
$$\left. \pm \frac{1-g}{p} \pm 2kg \right) f_s$$

Fig. 4 shows the spectral content of the voltage between sub-windings of dual three-phase induction motor under rotor construction asymmetry and non-uniform with a 30% static air-gap eccentricity.

In addition to the harmonics related to rotor construction asymmetry with frequencies $f_{sh}(1, k) = (3 - (3 \pm 1)g \pm 2kg)f_s$, one can notice the appearance of the first additional harmonics related to the static air-gap eccentricity at frequencies $f_{sh}(3, k) = (3 - (3 \pm 1)g \pm (1 - g) \pm 2kg)f_s$. Moreover, the interaction of the faulty part of mutual inductances with the healthy rotor current generates the second additional harmonics (23) at frequencies $f_{sh}(3(1+1), k) = (5 - (6 \pm 2)g \pm 2kg)f_s$ with a less effect.

5. Experimental validation

The dual three-phase induction motor is shown in Fig. 5. It is an adapted version of a three-phase 1.5-kW with 24 stator slots, 22 rotor bars, and 1 pair poles. Each sub-winding of motor is star-connected with the neutral accessible at the terminals. They were supplied directly from the power line and equipped with voltage probe. The load is a magnetic powder brake. The voltage between sub-windings of motor is measured for a different load and recorded by LeCroy scope (WR6050). The data were processed using the MATLAB software package to compute the fast Fourier transform (FFT) after the acquisition, and plot the neutral voltage spectra.

The top of Fig. 6 shows the spectrum of the voltage between sub-windings of tested motor operating with a slip $g = 0.0410$ under rotor construction dissymmetry and with residual static air-gap eccentricity. One can notice the appearance of the harmonics related to rotor construction dissymmetry at the following frequencies $f_{sh}(1, k) = (3 - (3 \pm 1)g \pm 2kg)f_s$ match to the simulation results Fig. 3, the unexpected harmonics with a less magnitude are those given for static air-gap eccentricity which means the existence of residual asymmetry in the air gap.

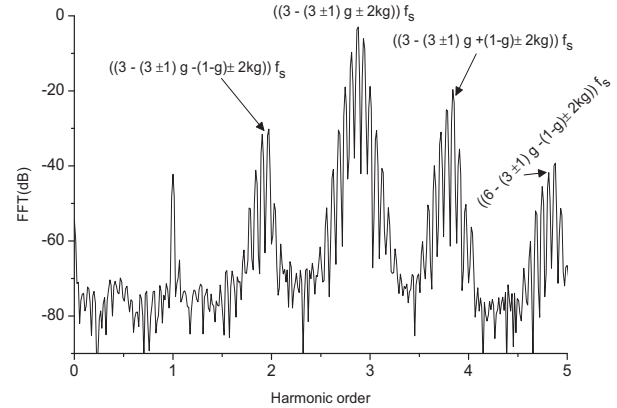To introduce the inherent static eccentricity, a ring with

Figure 4. Simulated normalized FFT spectrum of voltage between sub-windings of dual three-phase induction motor with rotor construction asymmetry and non-uniform static air-gap eccentricity.

Figure 5. Experimental setup for static air-gap eccentricity based on measuring of voltage between sub-windings of dual three-phase induction motor.
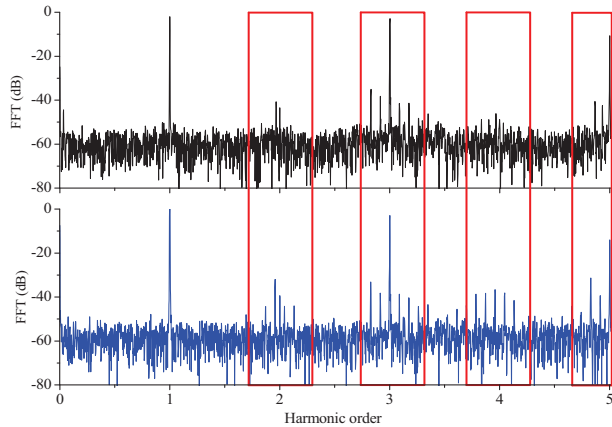
Figure 6. Experimental spectrum of voltage between sub-windings of dual three-phase induction motor with (top) residual static air-gap eccentricity and (bottom) 30% static air-gap eccentricity.

non-uniform thickness is inserted between the bearing and the end plate. The bottom of fig. 6 shows the spectrum of the voltage between sub-windings when the static air- gap eccentricity is introduced, additional components much greater related to the static air-gap eccentricity at frequencies described by (22) and (23).

6. Conclusion

This paper has investigated new diagnosis method based on measurements and frequency analysis of voltage between two sub-windings in dual three-phase induction motor. Special interest is focused on the rotor constructional asymmetry under uniform air-gap or non-uniform static air-gap eccentricity. It has been shown that the use of voltage between sub-winding of dual three-phase allows the prediction of the failures in the machine.

7. References

[1] L. Alberti and N. Bianchi "Experimental Tests of Dual Three-Phase Induction Motor Under Faulty Operating Condition", IEEE Trans. Ind. Electron., vol. 59, no. 5, May 2012.

[2] A. Boglietti , R. Bojoi , A. Cavagnino and A. Tenconi "Efficiency analysis of PWM inverter fed three-phase and dual three-phase high frequency induction machines for low/medium power applications", IEEE Trans. Ind. Electron., vol. 55, no. 5, pp: 2015-2023, 2008.

[3] K. Marouani, L. Baghli, D. Hadiouche, A. Kheloui, and A. Rezzoug,"A new PWM strategy based on a 24-sector vector space decomposition for a six-phase VSI-fed dual stator induction motor", IEEE Trans. Ind.Electron., vol. 55, no. 5, pp: 1910-1920, May 2008.

[4] D. Yazdani, S. Ali Khajehoddin, A. Bakhshai, and G. Joos, "Full utilization of the inverter in split-phase drives by means of a dual three-phase space vector classi?cation algorithm",IEEE Trans. Ind. Electron., vol. 56, no. 1, pp: 120-129, Jan. 2009.

[5] R. Andriamalala, H. Razik, L. Baghli, and F.-M. Sargos, "Eccentricity fault diagnosis of a dual-stator winding induction machine drive considering the slotting effects", IEEE Trans. Ind. Electron., vol. 55, no. 12, pp: 4238-4251, Dec. 2008.

[6] W. T. Thomson, D. Rankin, and D. G. Dorrell, "On-line current monitoring to diagnose airgap eccentricity in large three-phase induction motors?Industrial case histories verify the predictions", IEEE Trans.Energy Convers., vol. 14, no. 4, pp: 1372-1378, Dec. 1999.

[7] El Bouchikhi, E.H.; Choqueuse, V.; Benbouzid, M.; Charpentier, J.F. "Induction machine fault detection enhancement using a stator current high resolution spectrum", IECON 2012 - 38th Annual Conference on IEEE Ind. Electron. Society, pp: 3913-3918, 2012.

[8] G. M. Joksimovic, M. Duvoric, J. Penman, and N. Arthur, "Dynamic simulation of dynamic eccentricity in induction machines?Finding functionapproach",IEEE Trans. Energy Convers., vol. 15, no. 2, pp: 143-148, Jun. 2000.

[9] Dorrell, D.G. "Sources and Characteristics of Unbalanced Magnetic Pull in Three-Phase Cage Induction Motors With Axial-Varying Rotor Eccentricity", IEEE Trans. Ind. Appl. vol. 47, no. 1, pp: 12 - 24, Jan.-Feb. 2011

[10] C. Kral, F. Pirker, and G. Pascoli, "Rotor eccentricity detection of induction machines by means of torque estimation–Measurement results", inProc. IEEE SDEMPED, pp: 641-644, 2001.

[11] Drazen Dujic, Emil Levi and Martin Jones, "Dc Bus Utilisation in Multiphase VSI Supplied Drives with a Composite Stator Phase Number", Industrial Technology (ICIT), IEEE Conference on Industrial Technology, pp: 1495-1500, Viña del Mar, Chile, 2010,

[12] A. Khezzar, M. El Kamel Oumaamar, M. Hadjami, M. Boucherma, and H. Razik, "Induction motor diagnosis using line neutral voltage signatures", IEEE Trans. Ind. Electron., vol. 56, no. 11, pp: 4581-4591, Nov. 2009.